Acta Cryst F STRUCTURAL BIOLOGY COMMUNICATIONS
ISSN 2053-230X

Use of dynamic light scattering and small-angle X-ray scattering to characterize new surfactants in solution conditions for membrane-protein crystallization

Mohamed Dahani,[a] Laurie-Anne Barret,[a,b] Simon Raynal,[a] Colette Jungas,[b]‡ Pétra Pernot,[c] Ange Polidori[a] and Françoise Bonneté[a]*

[a]Institut des Biomolécules Max Mousseron/CBSA, UMR 5247, Avignon University, 33 Rue Louis Pasteur, 84000 Avignon,France, [b]Laboratoire de Bioénergétique Cellulaire/Biologie Végétale et Microbiologie Environnementales, UMR 7265, 13108 Saint-Paul-lez-Durance, France, and [c]European Synchrotron Radiation Facility, 71 Avenue des Martyrs, 38000 Grenoble, France. *Correspondence e-mail: francoise.bonnete@univ-avignon.fr

Received 16 March 2015
Accepted 18 May 2015

Edited by H. M. Einspahr, Lawrenceville, USA

‡ Present address: Laboratoire de Génétique et de Biophysique des Plantes (LGBP), UMR 7265 CNRS–CEA–AMU, Faculté des Sciences de Luminy, 163 Avenue de Luminy, 13009 Marseille, France.

Keywords: membrane protein; surfactant micelle; scattering techniques; phase diagram; crystallization.

The structural and interactive properties of two novel hemifluorinated surfactants, F_2H_9-β-M and F_4H_5-β-M, the syntheses of which were based on the structure and hydrophobicity of the well known dodecyl-β-maltoside (DD-β-M), are described. The shape of their micellar assemblies was characterized by small-angle X-ray scattering and their intermicellar interactions in crystallizing conditions were measured by dynamic light scattering. Such information is essential for surfactant phase-diagram determination and membrane-protein crystallization.

1. Introduction

The crystallization of membrane proteins (MPs) for structure resolution at the atomic level is a challenge in biocrystallography. MP structures represent less than 1% of the more than 100 000 structures deposited in the PDB. This deficit is caused by technically challenging steps: (i) large-scale MP production, (ii) the solubilization and purification of functionally stable MP complexes and (iii) the generation of crystals that diffract X-rays to high resolution. Without minimizing all of the previous essential biochemical steps, the crystallization of membrane proteins is a challenging task because amphiphilic molecules (namely surfactants) are ubiquitous in solution with membrane proteins, both bound to the protein and in micelle forms, which makes MP phase diagrams difficult to control (Nollert, 2005). Whereas well diffracting crystals can be obtained using the *in meso* crystallization method, *i.e.* by reconstitution in a lipidic environment, growing MP crystals directly *in surfo*, *i.e.* in micelles, remains the first and the most successful method used by structural biologists. Unfortunately, this method often results in poorly diffracting crystals. The difficulties in obtaining crystals that diffract X-rays to high resolution *via* the *in surfo* method can be attributed to different factors such as the instability of membrane proteins in detergent[1] and the sparsity of polar residues present on the surface of MPs, resulting in an insufficient number of crystalline lattice contacts. To overcome these difficulties, a critical

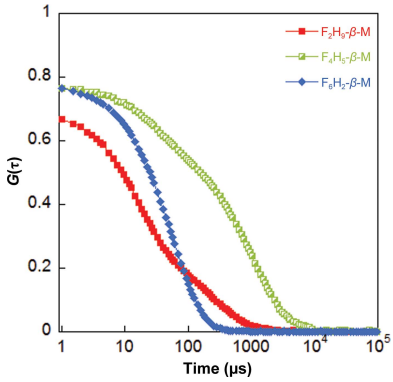

[1] Detergents are lipophilic surfactants that are able to solubilize lipid bilayers and extract MPs from membranes.

issue to consider is the selection of a detergent or other surfactant that will maintain the target MP in a stable, active and non-aggregated state. Stability is sometimes achieved with long-chain detergents, which form large micelles that are able to cover the hydrophobic transmembrane domain (Tate, 2010). For example, large micelle-forming detergents such as *n*-dodecyl-β-D-maltoside (DD-β-M) and nonaoxyethylene dodecyl ether ($C_{12}E_9$) are more likely to maintain an MP in solution by efficient shielding of the apolar surface of the MP. However, the large micellar size results in partial obstruction of the polar surface residues of the protein, thereby preventing the protein–protein interactions that are essential for crystal lattice formation. In contrast, small micelle detergents such as *n*-octyl-β-D-glucoside (β-OG) and *n*-octyl-β-D-maltoside (β-OM) leave more of the polar surface residues of the protein exposed to form the protein–protein contacts that are necessary for an ordered crystalline lattice. However, small micelle detergents may also inactivate MPs by intrusion of the detergent alkyl chain into the interior of the protein and/or by stripping away stabilizing lipids, cofactors or subunits. It is thus clear that detergent packing will significantly contribute to how complexes interact and self-assemble during phase transitions and how MPs are arranged within the crystalline lattice (Pebay-Peyroula *et al.*, 1995; Penel *et al.*, 1998). To overcome dissociative or destabilizing effects of detergents vis-à-vis MPs, different strategies have been developed over two decades to synthesize new surfactants (including *in vitro* synthesis; Park *et al.*, 2007; Nehmé *et al.*, 2010) to address the solubilization and purification (Duval-Terrié *et al.*, 2003; Yu *et al.*, 2000), trapping and stabilization (Chae *et al.*, 2012; Zhang *et al.*, 2011; Chae, Gotfryd *et al.*, 2010) of membrane proteins. Most of these new surfactants are valuable for solubilizing and stabilizing MPs, while the number of effective surfactants for crystallization and X-ray crystallography is rather limited. Among these new surfactants, maltose-neopentyl glycol-3 (MNG-3) enabled the crystallization of cytochrome b_6f to produce crystals that diffracted to a resolution similar to those obtained using the more usual DD-β-M (Chae, Rasmussen *et al.*, 2010). More recently, three-dimensional crystals of different families of MPs were obtained using steroid-based facial amphiphiles either alone or mixed with detergents or lipids (Lee *et al.*, 2013). However, crystallization successes are still rare because MP crystallization in surfactants is often considered to be a 'black art' in that the protocol involves screening several hundred potential conditions using a high-throughput methodology. While such screening strategies may sometimes lead to successful crystallization, the design of more efficient molecules requires understanding of the relationship between the amphiphile structure, the auto-assembly mechanism, the surfactant–protein interactions and the ability to promote availability of the lattice contacts required to crystallize MPs. In this context, we characterized the assembly properties of a new rigid surfactant, *trans*-propyl(bi)cyclohexyl-α-maltoside (PCC-α-M; Glycon), which was synthesized and described for MP stabilization and crystallization (Hovers *et al.*, 2011). In terms of the shape and size of the micelles, we showed that whereas DD-β-M and PCC-α-M present quite similar ellipsoidal shapes and sizes, the aggregation number (N_{agg}) is larger for PCC-α-M ($N_{agg} \simeq 165$) than for DD-β-M ($N_{agg} \simeq 125$) (Barret *et al.*, 2013). Moreover, the study of intermicellar interactions *via* measurement of the second virial coefficient (A_2) for rational crystallization showed PCC-α-M to be more attractive than DD-β-M, inducing a lower cloud-point boundary for PCC-α-M than for DD-β-M. Although the solubility of RC-LH1-pufX in this new surfactant was found to be lower and crystallization was found to be easier (Barret *et al.*, 2013), the diffraction quality was not increased sufficiently to make structure resolution possible, which is most likely to be the result of the detergent 'belt' surrounding the protein being too large (which is related to the higher aggregation number of PCC-α-M), therefore causing steric interference in the crystalline lattice. In an effort to improve MP crystallization and crystal packing, we synthesized new surfactants bearing a fluorinated segment on the hydrophobic chain. Fluorosurfactants have long been known to stabilize MPs without denaturation (Breyton *et al.*, 2004), being less intrusive and less delipidating than hydrogenated surfactants. Indeed, fluorocarbons are not miscible with water nor with hydrocarbons and are more bulky and rigid than hydrogenated surfactants (Barthélémy *et al.*, 2002). Therefore, to form small globular micelles (Polidori *et al.*, 2006; Breyton *et al.*, 2009) suitable for MP crystal growth, the length of the fluorinated segment must be adapted to the polar head size to reach an appropriate critical packing parameter (Israelachvili *et al.*, 1977). Based on the structure and hydrophobicity of DD-β-M, while supposing the rule that 1 $CF_2 \simeq 1.5$ CH_2 (Shinoda *et al.*, 1972; Ravey *et al.*, 1988), we have synthesized two new fluorinated surfactants, F_2H_9-β-M and F_4H_5-β-M (*i.e.* nine or five hydrogenated C atoms and two or four fluorinated C atoms, respectively, at the end of the chain). The physicochemical characteristics of micelle formation and their biochemical evaluation for the stabilization of membrane proteins have been thoroughly described by Polidori *et al.* (2015). In the present paper, we focus on the characterization of their micelle structures and intermicellar properties that may help in membrane-protein crystallization.

2. Materials and methods

2.1. Solutions for experiments

Dodecyl-β-maltoside (DD-β-M; <0.2% α anomer) and octyl fluorinated-β-maltoside (F_6H_2-β-M; <2% α anomer) were purchased from Anatrace. PCC-α-M was synthesized as described previously (Hovers *et al.*, 2011). F_2H_9-β-M and F_4H_5-β-M were synthesized at IBMM/CBSA, Avignon as described elsewhere (Polidori *et al.*, 2015). All surfactant stock solutions (between 50 and 100 mg ml^{-1} in water) were prepared 24 h prior to measurements in Milli-Q water filtered using 0.2 µ*M* Millipore filters followed by centrifugation at 15 000 rev min^{-1} for 2 h prior to transfer to clean measurement cells. For surfactant phase-diagram determination, monodisperse polyethylene glycol 3350 [50%(*w*/*v*) solution in water] was purchased from Hampton Research.

2.2. Dynamic light scattering (DLS)

Dynamic light-scattering experiments were performed at 20°C on a Zetasizer Nano-S model 1600 (Malvern Instruments, UK) equipped with an He–Ne laser (λ = 633 nm, 4.0 mW) at an angle of 173° (backscattering detection) in a 45 µl low-volume quartz cuvette. A total of five scans of 5 s duration were accumulated for each sample. The time-dependent correlation function $G(\tau)$ was measured for different concentrations of surfactants above their respective CMC in water using different percentages of PEG 3350 and was analysed either in cumulative mode if the distribution was monomodal [*i.e.* polydispersity index (PdI) < 20%] or in CONTIN mode if the distribution was multimodal (PdI > 20%) using the integrated *Zetasizer* software. The diffusion coefficient D_t was plotted as a function of surfactant concentration in order to obtain (i) the hydrodynamic radius (R_h) of the micelles from the intercept using the Stokes–Einstein equation $D_0 = k_B T/6\pi\eta R_h$, where k_B is Boltzmann's constant, T is the absolute temperature and η is the viscosity of the solvent, and (ii) the interaction parameter k_D (Li *et al.*, 2004) from the slope of $D_t = D_0[1 + k_D(c - \mathrm{CMC})]$. As for the second virial coefficient A_2 obtained from static light scattering or small-angle X-ray scattering, in the case where the micelle shape is independent of surfactant concentration, if k_D is positive the interactions between micelles are repulsive and if it is negative they are attractive.

2.3. Small-angle X-ray scattering

Micelle form factors of fluorosurfactants were characterized in water by small-angle X-ray scattering on the bioSAXS beamline ID14-eh3 and subsequently on BM29 (Pernot *et al.*, 2013) at the European Synchrotron Radiation Facility, Grenoble, France. Surfactant scattering patterns were measured at 20°C at several concentrations ranging from 2.5 to 40 mg ml^{-1} in H_2O. With a sample-to-detector distance of 2.425 m and an X-ray wavelength of 0.0931 nm, the achievable q-range was 0.05–4 nm^{-1}. To prevent radiation damage during the scattering experiments, data were collected in ten successive 2 s frames and the solution flowed in the capillary during exposure. Averaged scattered intensities were water-scattering subtracted and normalized to the surfactant concentration. Forward scattering values (*i.e.* $q \rightarrow 0$) $I(c, 0)/c$ and radii of gyration R_g were evaluated using the Guinier approximation $I(c, q) = I(0)\exp(-q^2R_g^2/3)$ assuming that $qR_g < 1$ at very small angles. The micelle molar mass and aggregation number of the surfactants were then calculated from the absolute forward intensity normalized to a reference of pure water (Orthaber *et al.*, 2000). The aggregation number N_{agg} was determined by dividing the micelle mass by that of the surfactant monomer,

$$N_{agg} = N_a \frac{I(0)_{mic}}{M_{surf}(c - \mathrm{CMC})I(0)_{water}[r_0\overline{v}_p(\rho_{surf} - \rho^\circ)]^2}\left.\frac{d\Sigma}{d\Omega}\right|_{water}, \quad (1)$$

where N_a is Avogadro's number, r_0 is the classical electron radius (r_0 = 0.28179 × 10^{-12} cm e^{-1}), $\overline{v}_p$ is the measured surfactant specific volume (in cm^3 g^{-1}), M_{surf} is the surfactant molar mass, ρ_{surf} and ρ° are the scattering-length densities of the surfactant and water (in e$^-$ cm^{-3}), respectively, and $\left.\frac{d\Sigma}{d\Omega}\right|_{water}$ is the absolute scattering intensity of water, which is equal to 0.01632 cm^{-1} at 20°C.

The maximum particle dimension, D_{max}, and the pair distribution function, $P(r)$, were finally determined by inverse Fourier transformation using the program *GNOM* (Svergun, 1992) to evaluate the geometry of the micelles.

Table 1
Surfactant parameters.

Surfactant (No. C/eq. C)†	Formula	Formula weight (Da)	CMC‡ (mM g l^{-1})	$\overline{v}_p$ (ml g^{-1})	ρ_{surf} (e$^-$ cm^{-3})
PCC-α-M (15C)	$C_{27}H_{48}O_{11}$	548.66	0.036/0.02	0.799	0.409
DD-β-M (12C)	$C_{24}H_{46}O_{11}$	510.60	0.17/0.08	0.819	0.400
F_2H_9-β-M (11C/12C)	$C_{23}H_{39}F_5O_{11}$	586.54	1.14/0.67	0.749	0.425
F_4H_5-β-M (9C/11C)	$C_{21}H_{31}F_9O_{11}$	630.45	2.16/1.36	0.632	0.493
F_6H_2-β-M (8C/11C)	$C_{20}H_{25}F_{13}O_{11}$	688.40	0.71/0.49	0.578	0.529

† No. C corresponds to the number of carbons on the chain and eq. C corresponds to the number of C assuming that 1CF2 = 1.5CH2. ‡ From surface tensiometry (Polidori *et al.*, 2015).

2.4. Density and partial specific volume measurements

Surfactant specific volume (in cm^3 g^{-1}) was calculated from the precise measurement at 20°C (using an Anton-Paar DMA4500M density meter) of ρ and ρ°, which are the densities of surfactant solutions at different concentrations ranging from 0.2 to 10 mg ml^{-1} and of H_2O, respectively. The surfactant stock solutions were prepared by precisely weighting both the surfactant and the solvent at about 10 mg ml^{-1}. Surfactant solutions were obtained by successive dilutions from stock solutions. The specific volume was then obtained from the slope of the equation

$$\frac{\rho_{surf} - \rho^\circ}{c} = 1 - \overline{v}_p\rho^\circ. \quad (2)$$

2.5. Cloud-point boundary

Surfactant phase diagrams were determined by optical microscopy visualization (Carl Zeiss SteREO Discovery.V12 microscope). 10 µl droplets of a mixture of 2–10% PEG 3350 and 5–50 mg ml^{-1} surfactant in water were deposited in microbatch plates and immediately observed. For each PEG concentration, the surfactant concentration was increased by 1 mg ml^{-1} stepwise until a phase transition was observed.

3. Results and discussion

Two new fluorinated surfactants, *i.e.* F_2H_9-β-M and F_4H_5-β-M, derived from the well known DD-β-M, bearing either a short perfluoroethyl or perfluorobutyl tip at the end of the aliphatic chain, are presented in Fig. 1. Their micellar properties in terms of CMC (Table 1), micellization behaviour, micelle homogeneity and biochemical evaluation for the stabilization

of membrane proteins have been thoroughly described and compared with those of both fully hydrogenated DD-β-M and perfluorinated F_6H_2-β-M (Polidori *et al.*, 2015). Here, we evaluate their interest for membrane-protein crystallization by describing their micellar assemblies and interactive properties. Since the pioneering work of Loll and coworkers (Hitscherich *et al.*, 2000), it is now recognized that the behaviour of protein-free micelles, in particular the existence of attractive interactions between micelles and the location of the surfactant phase boundary in the phase diagram, is a good predictor of the crystallization of protein–surfactant complexes (PSCs; Berger *et al.*, 2006; Hitscherich *et al.*, 2001; Koszelak-Rosenblum *et al.*, 2009; Loll *et al.*, 2001). However, the growth of PSC crystals suitable for X-ray diffraction using the *in surfo* method depends not only on stable monodisperse PSCs but also on small homogeneous surfactant micelles that favour protein–protein contacts in the crystal lattice. We have therefore characterized the sizes, shapes and the interactions between micelles of the two novel fluorosurfactants by small-angle X-ray scattering and dynamic light scattering in water and in crystallization conditions that could be helpful for MP crystallization.

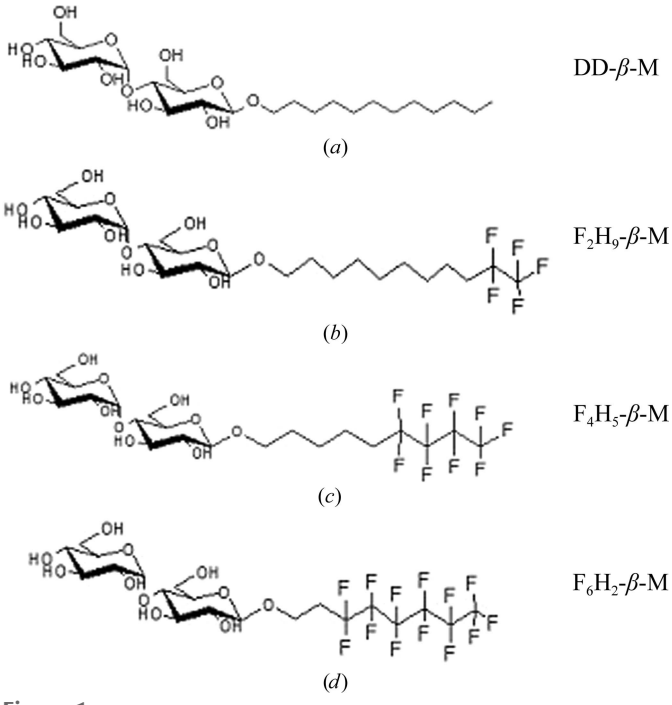

Figure 1
Chemical structures of surfactants: DD-β-M (*a*), F_2H_9-β-M (*b*), F_4H_5-β-M (*c*) and F_6H_2-β-M (*d*).

3.1. Fluorinated surfactant behaviour in water

3.1.1. Dynamic light scattering. Dynamic light scattering (DLS) is routinely used in crystallization to detect aggregates in solution, to evaluate the polydispersity of solutions and to determine the size of particles or macromolecules in solution. It can be also used to characterize weak interactions between particles (Li *et al.*, 2004) prior to crystallization.

We have performed dynamic light-scattering experiments on the two new fluorosurfactants F_2H_9-β-M and F_4H_5-β-M in H_2O at different concentrations and compared then with the hydrogenated DD-β-M and the perfluorinated F_6H_2-β-M. Fig. 2 shows examples of the correlation function (Fig. 2*a*), the size distribution in intensity (Fig. 2*b*) and the size distribution in volume (Fig. 2*c*) for the three fluorosurfactants at about 20× CMC.

Although large aggregates (>100 nm) appear in the size distribution in intensity for F_2H_9-β-M and F_4H_5-β-M, their contribution (intensity $\propto R^6$) is negligible as seen from the

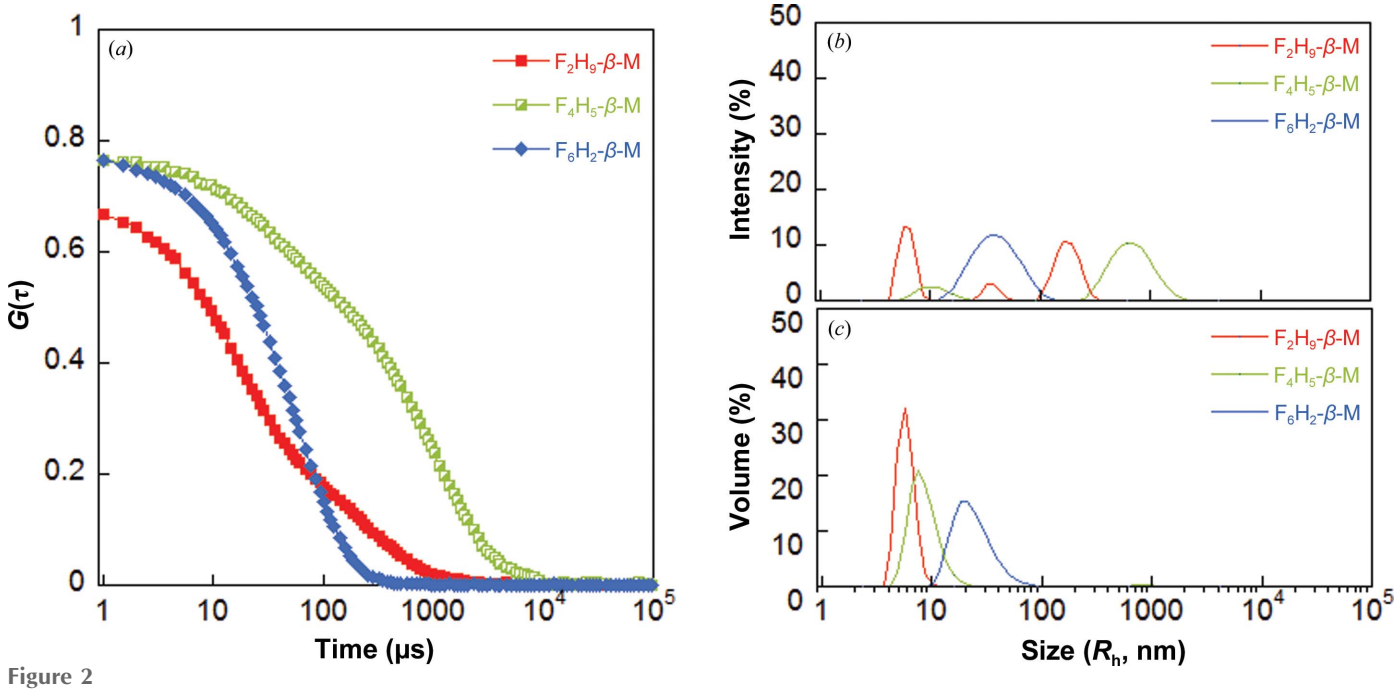

Figure 2
Autocorrelation functions and size distributions of F_2H_9-β-M, F_4H_5-β-M and F_6H_6-β-M at 20× CMC in water.

Table 2
Structural characteristics of surfactant micelles from SAXS and DLS.

	Data from SAXS						Data from DLS		
Surfactant	Concentration (g l^{-1})	$I(0)/c$ − CMC (cm^2 g)	R_g (nm)	D_{max} (nm)	$L = (12R_g/R_c)^{1/2}$ (nm)	N_{agg}	Concentration (g l^{-1})	D_t (μ^2 s^{-1})	PdI
DD-β-M†	2.5	24.7	3.2	8.0		125	10	60.2	0.13
							20	61.9	0.09
							30	60.9	0.08
							40	59.9	0.11
							50	60.1	0.07
							70	56.3	0.17
							100	57.2	0.04
F_2H_9-β-M	2.5	21.41	2.57	8.9		60	20	73.6	0.60
	5	22.93	2.54	7.3		65	30	64.7	0.70
	10	23.22	2.50	7.6		65	40	62.8	0.66
	20	23.84	2.48	6.5		67	50	57.9	0.55
	40	20.53	2.37	8.2		58			
F_4H_5-β-M	2.5	31.75	6.17	17.2		38	12	47.1	0.89
	5	25.93	3.37	10.2		31	27	43.9	1.00
	10	33.10	3.22	10.8		40	41	42.3	1.00
	20	36.47	3.54	10.1		44	54	40.1	0.99
	40	43.43	3.79	10.9		52	85	37.7	0.95
							100	35.9	0.18
F_6H_2-β-M	1.5	728.82	12.38	NA	42.9/1.86	625	13	13.0	0.19
	3.1	936.62	13.78	55	47.7/1.66	803	28	12.9	0.21
	6.2	945.76	15.21	56	52.7/1.64	811	35	12.2	0.22
	12.5	903.22	15.81	57	54.8/1.63	774	42	11.7	0.21
	25	746.43	14.76	59	51.1/1.62	640	50	11.2	0.24
	50	530.67	12.91	58.6	44.7/1.58	455	70	10.2	0.30

† From Barret *et al.* (2013).

distribution in volume (<1%). The hydrodynamic radius R_h of the fluorosurfactant micelles was thus determined by extrapolation to zero concentration of $D_t = f(c - \text{CMC})$ (Fig. 3) for the major distribution peak. We observe that R_h increases as the length of the fluorinated segment increases (inserted table in Fig. 3), although the total number of C atoms (*i.e.* the chain length) decreases. This is the opposite of what is observed with alkyl chains (Meyer *et al.*, 2015; Oliver *et al.*, 2013), where the micelle size increases as the chain length increases.

The micelle size of fluorosurfactants seems to be influenced by the length of the fluorinated segment. With a small segment, F_2H_9-β-M behaves as an alkyl chain with 11 C atoms. Micelles of F_2H_9-β-M are smaller than micelles of DD-β-M (H_{12}-β-M), whereas for F_4H_5-β-M and F_6H_2-β-M the micelle size seems to be more influenced by the rigidity and bulkiness of the fluorinated segment than by the length of the chain. With a long fluorinated chain and a linear maltoside head, F_6H_2-β-M forms elongated micelles as expected from the packing parameter (Israelachvili *et al.*, 1977) and as recently described (Frotscher *et al.*, 2015). The only particular behaviour could be for F_4H_5-β-M, which is composed of half hydrogenated and half fluorinated C atoms and for which the immiscibility of fluorine and hydrogen could confer instability in micelle assembly. This behaviour has been thoroughly described elsewhere in terms of micellization thermodynamics (Polidori *et al.*, 2015). However, for each surfactant the diffusion coefficient D_t decreases as the surfactant concentration increases, which could be attributed either to attractive intermicellar interactions ($k_D < 0$) or to an increase in micelle size. To discriminate between the two behaviours, SAXS experiments were performed on each surfactant in water as a function of concentration.

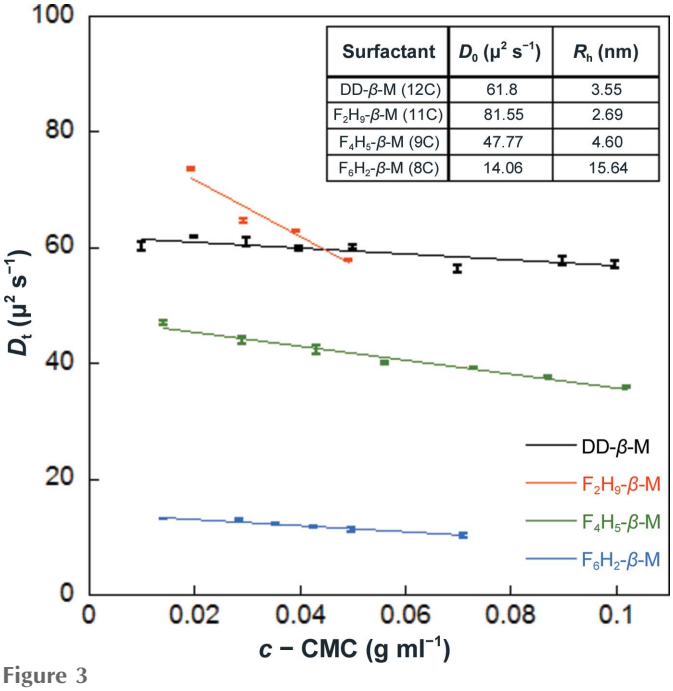

Figure 3
The diffusion coefficient as a function of concentration for the four surfactants in water.

3.1.2. Small-angle X-ray scattering. SAXS is a suitable tool to characterize the structure and form factors of macromolecules and particles in solution. To discriminate between interactions between micelles and the change in micelle size as observed by DLS, SAXS experiments were performed with each surfactant in water as a function of concentration. Fig. 4 depicts the SAXS patterns for F_2H_9-β-M, F_4H_5-β-M and F_6H_2-β-M, the forward intensities for determination of molar mass and aggregation number and the pair distribution function, $P(r)$, as a function of surfactant concentration. The structural parameters (R_g, D_{max} and N_{agg}) obtained from SAXS analysis are presented in Table 2.

F_2H_9-β-M and F_6H_2-β-M present a stable shape at concentrations above 6–8× CMC, as seen over a large q-range ($q > 0.5$ nm^{-1}). While F_2H_9-β-M seems to form small almost globular micelles with $N_{agg} \simeq 65$ (*i.e.* molar mass $\simeq 38\,000 \pm 1000$ g mol^{-1}), F_6H_2-β-M forms large elongated (rod-like) micelles from the log–log representation with an N_{agg} of

greater than 800 (*i.e.* molar mass $\simeq$ 550 000 $\pm$ 5000 g mol^{-1}). In contrast, F_4H_5-β-M exhibits an evolution in the SAXS curves probably owing to an evolution in micellization as observed by DLS. The molar masses of the micelles are found to be between 20 000 and 32 000 g mol^{-1}. The maximum distances, D_{max}, for the three fluorosurfactants obtained from the SAXS pair distribution function (Figs. 4*g*, 4*h* and 4*i*) are in agreement with the values of the hydrodynamic radius obtained from DLS experiments. Both F_2H_9-β-M and F_6H_2-β-M present overall repulsive interactions, as seen from the decrease in normalized forward intensity as a function of concentration (Figs. 4*d* and 4*f*) when the micelle shape is stable. The second virial coefficients A_2 were characterized. We thus found that A_2 is $+0.7 \times 10^{-4}$ mol ml g^{-2} for F_2H_9-β-M and $+0.08 \times 10^{-4}$ mol ml g^{-2} for F_6H_2-β-M in water, with the decrease in the repulsive contribution of the second virial coefficient being owing to an increase in the micelle size (Tanford, 1961). The change observed in D_t for F_2H_9-β-M and F_6H_2-β-M can therefore be attributed to interactions between micelles, as was observed for DD-β-M (Barret *et al.*, 2013). The decrease in D_t of F_4H_5-β-M may, in contrast, be correlated to the increase in micelle size. We calculated $K_D = k_D/M$ for comparison with A_2 from SAXS. We found that K_D is -0.62 mol ml g^{-2} for F_2H_9-β-M and -0.01 mol ml g^{-2} for F_6H_2-β-M. As previously reported in the literature (Harding & Johnson, 1985), the values of K_D obtained by DLS are lower than the values of A_2 obtained from static measurements (SAXS or SLS) owing to hydrodynamic contributions. Despite this discrepancy, the interaction parameters obtained from DLS experiments could be used to characterize the properties of surfactant micelles in solution conditions for MP crystallization.

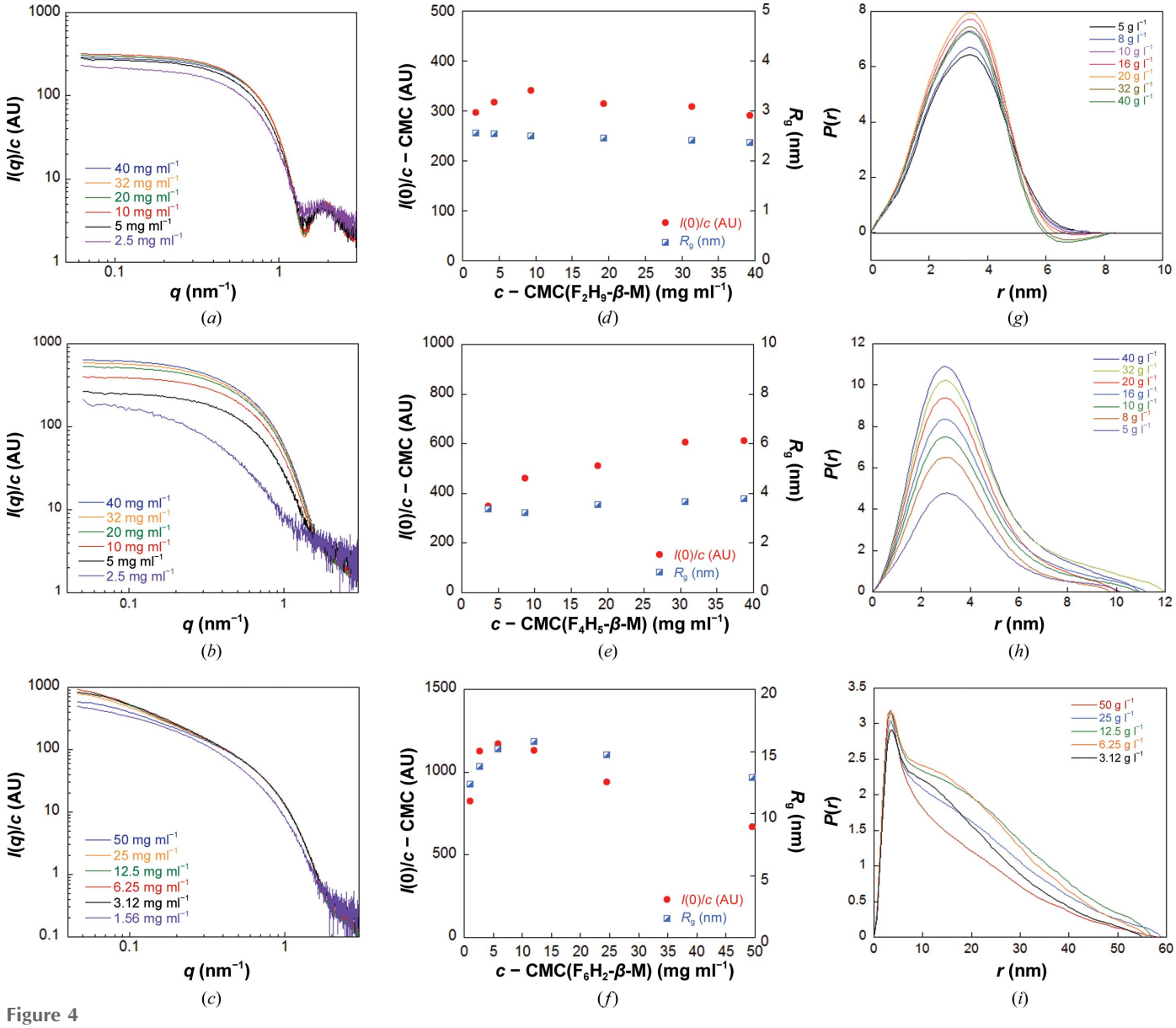

Figure 4
SAXS experiments in water. Left column, SAXS patterns; middle column, normalized forward intensities as a function of surfactant concentration; right column, pair distribution functions. Top row, F_2H_9-β-M; middle row, F_4H_5-β-M; bottom row, F_6H_2-β-M.

3.1.3. Interactions by DLS in PEG solutions. Interactions between micelles in solution conditions for membrane-protein crystallization have mainly been studied by measurement of the second virial coefficient (A_2 or B_{22}) using, for example, static light scattering or small-angle X-ray scattering (Barret *et al.*, 2013; Hitscherich *et al.*, 2000). Such methods are time-consuming and require calibration, proper solvent subtraction and concentration normalization. Without solvent subtraction or calibration to analyse the polydispersity and size distribution of particles in solution, dynamic light scattering is increasingly being used to characterize interaction parameters (Saluja *et al.*, 2010; Shi *et al.*, 2013; Yadav *et al.*, 2011). In order to validate DLS measurements for MP crystallization diagnostics, experiments were initially performed in DD-β-M and PCC-α-M and compared with our previous SAXS studies (Barret *et al.*, 2013). The variation of the diffusion coefficient ratio D_t/D_0 is linear, since $D_t/D_0 = 1 + MK_D(c - \mathrm{CMC})$, and decreases as the concentration of surfactant increases (Fig. 5*a*), suggesting attractive interactions ($K_D < 0$) between PCC-α-M micelles. The slope K_D increases as the percentage of PEG 3350 increases owing to a depletion mechanism of the polymer (Asakura & Oosawa, 1958). The interaction parameters K_D for DD-β-M and PCC-α-M are plotted as a function of the percentage of PEG 3350 and compared with the second virial coefficient A_2 as measured by SAXS (Fig. 5*b*; Barret *et al.*, 2013). The variation in K_D follows the same trend as A_2 for the two surfactants, *i.e.* an increase in intermicellar attraction as the percentage of PEG increases, with the K_D values being lower than the A_2 values for the two surfactants, as observed for FH-β-M in water.

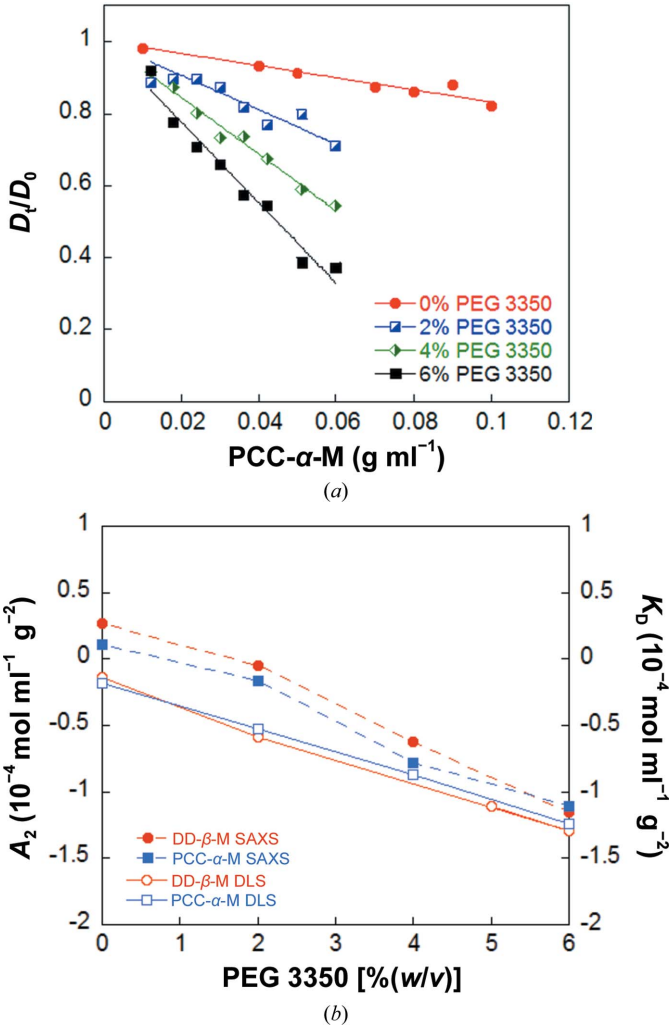

Figure 5
(*a*) DLS experiments on PCC-α-M as a function of the percentage of PEG 3350 for the determination of interaction parameters. (*b*) Comparison of $K_D = k_D/M$ from DLS and A_2 from SAXS for DD-β-M and PCC-α-M.

3.2. Interactions for cloud-point boundary

Membrane proteins are often observed to crystallize close to the detergent cloud-point boundary (Wiener & Snook, 2001), which corresponds to strong intermicellar attractions (Vivarès & Bonneté, 2004; Loll *et al.*, 2001). With this in mind, we have characterized interactions between fluorinated micelles by determining the interaction parameter K_D by DLS for the two fluorinated surfactants which present the most

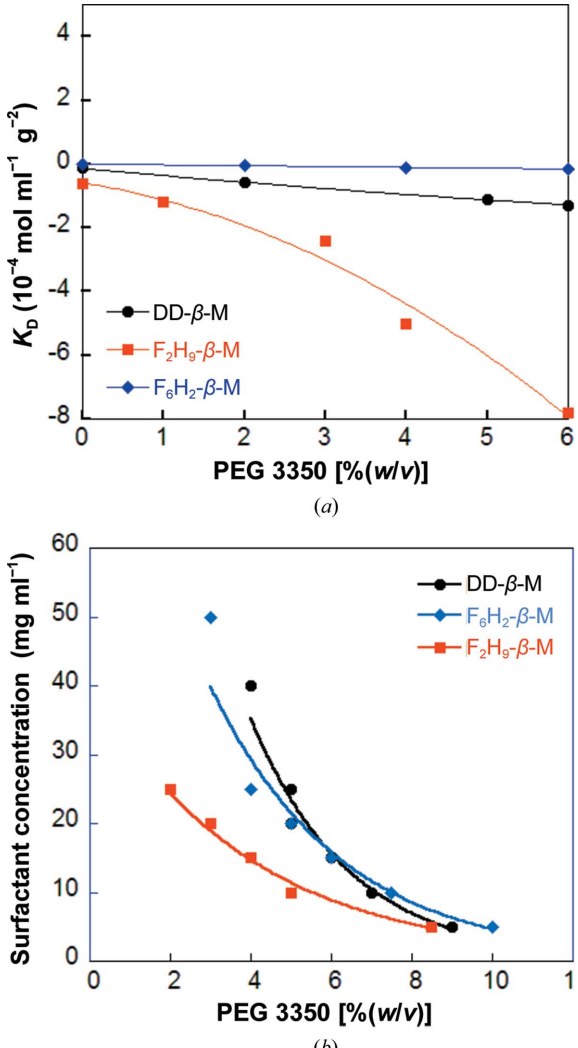

Figure 6
Interactions and cloud-point boundary of F_2H_9-β-M and F_6H_2-β-M compared with DD-β-M.

stable forms, *i.e.* F_2H_9-β-M and F_6H_2-β-M, as a function of concentration and compared them with that of DD-β-M. Fig. 6(*a*) shows the variation of K_D as a function of the percentage of PEG 3350. As expected from the depletion effect, interactions between micelles become more attractive ($K_D < 0$) as the polymer concentration increases, with the overall interactions being more attractive with F_2H_9-β-M than with F_6H_2-β-M or DD-β-M, in part owing to an increase in hard sphere potential and possible sugar-head hydration forces (Bauer *et al.*, 2012) for F_6H_2-β-M. A similar trend is observed in the cloud-point boundary (Fig. 6*b*) for the two surfactants compared with DD-β-M. The liquid–liquid phase transition is observed by optical microscopy at lower concentrations of surfactant and polymer for F_2H_9-β-M than for F_6H_2-β-M or DD-β-M. This result may be helpful for MP crystallization. Indeed, while a close correlation between solubility and second virial coefficient has long been demonstrated (Guo *et al.*, 1999), the correlation of second virial coefficients between surfactant micelles on one hand and membrane protein–surfactant complexes on the other highlighted by Loll and coworkers (Hitscherich *et al.*, 2000; Loll *et al.*, 2001), as well as our recent results on free micelles and on the RC-LH1-pufX complex with PCC-α-M (Barret *et al.*, 2013), suggest that a membrane protein purified in F_2H_9-β-M would have a lower solubility than one purified in DD-β-M.

4. Conclusion

Crystallization of membrane proteins in surfactant micelles suffers from a lack of fundamental studies to decipher the mechanisms, which could improve success in the growth of strongly diffracting crystals. Since the pioneering work of Loll and coworkers (Hitscherich *et al.*, 2000), mechanistic studies have mainly dealt with traditional hydrogenated detergents. There is a lack of studies for some of the newer amphiphilic molecules that promote membrane-protein crystallization. In the present paper, we have assessed the potential of new fluorinated surfactants for MP crystallization by describing their structure and interactions in crystallizing solutions. It appears that a surfactant such as F_2H_9-β-M, which forms small stable micelles in an attractive regime in the presence of crystallizing agent while at the same time stabilizing MP, could be a good candidate for crystallization, as previously observed for PCC-α-M (Barret *et al.*, 2013). However, comparison of these two surfactants, which form more attractive micelles than DD-β-M but with different aggregation numbers, raises an important question regarding the influence of the aggregation number on the amount of surfactant associated with the protein and its effect on crystal quality. Finally, the synthesis of a large amount of any new compound for MP stabilization and crystallization is not trivial. Since a thorough description of the surfactant micelle is a prerequisite for any surfactant exchange and membrane protein–surfactant complex crystallization, future studies in our laboratory will focus on large-scale synthesis of F_2H_9-β-M for MP crystallization trials and for comparison with other surfactants.

Acknowledgements

This study was supported by a PhD grant from the PACA region (Provence–Alpes–Cote d'Azur, France) *via* European Regional Development funds (FEDER). We are grateful to the European Synchrotron Radiation Facility for provision of synchrotron-radiation facilities and Adam Round for assistance in using beamlines ID14-eh3 and BM29.

References

Asakura, S. & Oosawa, F. (1958). *J. Polym. Sci.* **33**, 183–192.
Barret, L.-A., Barrot-Ivolot, C., Raynal, S., Jungas, C., Polidori, A. & Bonneté, F. (2013). *J. Phys. Chem. B*, **117**, 8770–8781.
Barthélémy, P., Tomao, V., Selb, J., Chaudier, Y. & Pucci, B. (2002). *Langmuir*, **18**, 2557–2563.
Bauer, C., Bauduin, P., Girard, L., Diat, O. & Zemb, T. (2012). *Colloids Surf. A Physicochem. Eng. Asp.* **413**, 92–100.
Berger, B. W., Gendron, C. M., Lenhoff, A. M. & Kaler, E. W. (2006). *Protein Sci.* **15**, 2682–2696.
Breyton, C., Chabaud, E., Chaudier, Y., Pucci, B. & Popot, J.-L. (2004). *FEBS Lett.* **564**, 312–318.
Breyton, C., Gabel, F., Abla, M., Pierre, Y., Lebaupain, F., Durand, G., Popot, J.-L., Ebel, C. & Pucci, B. (2009). *Biophys. J.* **97**, 1077–1086.
Chae, P. S., Gotfryd, K., Pacyna, J., Miercke, L. J. W., Rasmussen, S. G. F., Robbins, R. A., Rana, R. R., Loland, C. J., Kobilka, B., Stroud, R., Byrne, B., Gether, U. & Gellman, S. H. (2010). *J. Am. Chem. Soc.* **132**, 16750–16752.
Chae, P. S., Rasmussen, S. G. F. *et al.* (2010). *Nature Methods*, **7**, 1003–1008.
Chae, P. S., Rasmussen, S. G. F., Rana, R. R., Gotfryd, K., Kruse, A. C., Manglik, A., Cho, K. H., Nurva, S., Gether, U., Guan, L., Loland, C. J., Byrne, B., Kobilka, B. K. & Gellman, S. H. (2012). *Chem. Eur. J.* **18**, 9485–9490.
Duval-Terrié, C., Cosette, P., Molle, G., Muller, G. & Dé, E. (2003). *Protein Sci.* **12**, 681–689.
Frotscher, E., Danielczak, B., Vargas, C., Meister, A., Durand, G. & Keller, S. (2015). *Angew. Chem. Int. Ed.* **54**, 5069–5073.
Guo, B., Kao, S., McDonald, H., Asanov, A., Combs, L. L. & Wilson, W. W. (1999). *J. Cryst. Growth*, **196**, 424–433.
Harding, S. E. & Johnson, P. (1985). *Biochem. J.* **231**, 543–547.
Hitscherich, C. J., Allaman, M., Wiencek, J., Kaplan, J. & Loll, P. J. (2000). *Protein Sci.* **9**, 1559–1566.
Hitscherich, C., Aseyev, V., Wiencek, J. & Loll, P. J. (2001). *Acta Cryst.* D**57**, 1020–1029.
Hovers, J. *et al.* (2011). *Mol. Membr. Biol.* **28**, 171–181.
Israelachvili, J. N., Mitchell, D. J. & Ninham, B. W. (1977). *Biochim. Biophys. Acta*, **470**, 185–201.
Koszelak-Rosenblum, M., Krol, A., Mozumdar, N., Wunsch, K., Ferin, A., Cook, E., Veatch, C. K., Nagel, R., Luft, J. R., DeTitta, G. T. & Malkowski, M. G. (2009). *Protein Sci.* **18**, 1828–1839.
Lee, S. C., Bennett, B. C., Hong, W.-X., Fu, Y., Baker, K. A., Marcoux, J., Robinson, C. V., Ward, A. B., Halpert, J. R., Stevens, R. C., Stout, C. D., Yeager, M. J. & Zhang, Q. (2013). *Proc. Natl Acad. Sci. USA*, **110**, E1203–E1211.
Li, S., Xing, D. & Li, J. (2004). *J. Biol. Phys.* **30**, 313–324.
Loll, P. J., Allaman, M. & Wiencek, J. (2001). *J. Cryst. Growth*, **232**, 432–438.
Meyer, A., Dierks, K., Hussein, R., Brillet, K., Brognaro, H. & Betzel, C. (2015). *Acta Cryst.* F**71**, 75–81.
Nehmé, R., Joubert, O., Bidet, M., Lacombe, B., Polidori, A., Pucci, B. & Mus-Veteau, I. (2010). *Biochim. Biophys. Acta*, **1798**, 1100–1110.
Nollert, P. (2005). *Prog. Biophys. Mol. Biol.* **88**, 339–357.
Oliver, R. C., Lipfert, J., Fox, D. A., Lo, R. H., Doniach, S. & Columbus, L. (2013). *PLoS One*, **8**, e62488.
Orthaber, D., Bergmann, A. & Glatter, O. (2000). *J. Appl. Cryst.* **33**, 218–225.

Park, K.-H., Berrier, C., Lebaupain, F., Pucci, B., Popot, J.-L., Ghazi, A. & Zito, F. (2007). *Biochem. J.* **403**, 183–187.
Pebay-Peyroula, E., Garavito, R., Rosenbusch, J., Zulauf, M. & Timmins, P. (1995). *Structure*, **3**, 1051–1059.
Penel, S., Pebay-Peyroula, E., Rosenbusch, J., Rummel, G., Schirmer, T. & Timmins, P. A. (1998). *Biochimie*, **80**, 543–551.
Pernot, P. *et al.* (2013). *J. Synchrotron Rad.* **20**, 660–664.
Polidori, A., Presset, M., Lebaupain, F., Ameduri, B., Popot, J.-L., Breyton, C. & Pucci, B. (2006). *Bioorg. Med. Chem. Lett.* **16**, 5827–5831.
Polidori, A., Raynal, S., Barret, L.-A., Dahani, M., Barrot-Ivolot, C., Jungas, C., Keller, S., Ebel, C., Breyton, C. & Bonneté, F. (2015). In preparation.
Ravey, J.-C., Gherbi, A. & Stébé, M.-J. (1988). *Prog. Colloid Polym. Sci.* **76**, 234–241.
Saluja, A., Fesinmeyer, R. M., Hogan, S., Brems, D. N. & Gokarn, Y. R. (2010). *Biophys. J.* **99**, 2657–2665.
Shi, S., Uchida, M., Cheung, J., Antochshuk, V. & Shameem, M. (2013). *Int. J. Biol. Macromol.* **62**, 487–493.
Shinoda, K., Hato, M. & Hayashi, T. (1972). *J. Phys. Chem.* **76**, 909–914.
Svergun, D. I. (1992). *J. Appl. Cryst.* **25**, 495–503.
Tanford, C. (1961). *Physical Chemistry of Macromolecules.* New York: Wiley.
Tate, C. G. (2010). *Methods Mol. Biol.* **601**, 187–203.
Vivarès, D. & Bonneté, F. (2004). *J. Phys. Chem. B*, **108**, 6498–6507.
Wiener, M. C. & Snook, C. F. (2001). *J. Cryst. Growth*, **232**, 426–431.
Yadav, S., Scherer, T. M., Shire, S. J. & Kalonia, D. S. (2011). *Anal. Biochem.* **411**, 292–296.
Yu, S. M., McQuade, D. T., Quinn, M. A., Hackenberger, C. P. R., Gellman, S. H., Krebs, M. P. & Polans, A. S. (2000). *Protein Sci.* **9**, 2518–2527.
Zhang, Q., Tao, H. & Hong, W.-X. (2011). *Methods*, **55**, 318–323.